

# Extended logistic growth model for heterogeneous populations

Wang Jin<sup>1</sup>, Scott W McCue<sup>1</sup>, \*Matthew J Simpson<sup>1</sup>

<sup>1</sup> *School of Mathematical Sciences, Queensland University of Technology (QUT)  
Brisbane, Queensland, Australia.*

---

## Abstract

Cell proliferation is the most important cellular-level mechanism responsible for regulating cell population dynamics in living tissues. Modern experimental procedures show that the proliferation rates of individual cells can vary significantly within the same cell line. However, the standard approach to model cell proliferation in the mathematical biology literature is to use a classical logistic equation which neglects variations in the proliferation rate. In this work we consider a discrete mathematical model of cell migration and cell proliferation, modulated by volume exclusion (crowding) effects, with heterogeneity in the rates of proliferation of individual cells within the population. Constructing the continuum limit of the discrete model leads to a generalisation of the classical logistic growth model. Comparing numerical solutions of the model to averaged data from discrete simulations shows that the new model captures the key features of the discrete process. Applying the extended logistic model to simulate a proliferation assay using rates from recent experimental literature shows that neglecting the role of heterogeneity can lead to misleading results.

*Key words:* Cell proliferation, Heterogeneity, Population dynamics, Logistic growth.

## 1 Introduction

2 Cell proliferation is essential for regulating the dynamics of cell populations,  
3 and plays a vital role in collective cell spreading, cancer progression and tissue  
4 regeneration (Eladdadi and Isaacson, 2008; Evan and Vousden, 2001; Haridas  
5 et al., 2017; Pavlath et al., 1998). While it is clear that cells from different  
6 cell lines proliferate at different rates (Hayflick, 1965), recent experimental  
7 methods indicate that heterogeneity in cell proliferation arises even within  
8 the same cell line (Bajar et al., 2016; Guan et al., 2014; Sakaue-Sawano et al.,  
9 2008).

10 Many different types of experiments are used to quantify cell proliferation  
11 (An et al., 2001; Azzarone and Macieira-Coelho, 1982; Haass et al., 2014;  
12 Hayflick, 1965; Jin et al., 2017; Kaneoka et al., 1983; Willaime et al., 2013). The  
13 complexity of these experiments varies from simple *in vitro* proliferation assays  
14 in which the net expansion of a population of cells is observed and measured,  
15 such as the experiment shown in Figure 1, to more sophisticated experiments  
16 that use fluorescent cell cycle indicators to measure the duration of different  
17 phases of the cell cycle for individual cells (Bajar et al., 2016; Haass et al.,  
18 2014; Sakaue-Sawano et al., 2008). A standard measure of cell proliferation is  
19 the doubling time, which is a measure of the duration of time required for a  
20 population of cells, at low density, to double (Hayflick, 1965; Jin et al., 2016).  
21 The doubling time quantifies cell proliferation from the perspective of the  
22 entire population, and any kind of variability amongst individual cells in the  
23 population is neglected. Modern experimental approaches, such as individual-  
24 level fluorescent cell cycle indicators and micro collagen gel arrays, allow us  
25 to quantify variations in the cell cycle of individual cells (Guan et al., 2014;  
26 Haass et al., 2014). This individual-level data shows that proliferation rates

---

\* Corresponding author

*Email address:* [matthew.simpson@qut.edu.au](mailto:matthew.simpson@qut.edu.au), *Telephone* + 61 7 31385241,  
*Fax* + 61 7 3138 2310 (Wang Jin<sup>1</sup>, Scott W McCue<sup>1</sup>, \*Matthew J Simpson<sup>1</sup>).

27 of individual cells can vary significantly within the same cell line (Guan et al.,  
28 2014; Haass et al., 2014).

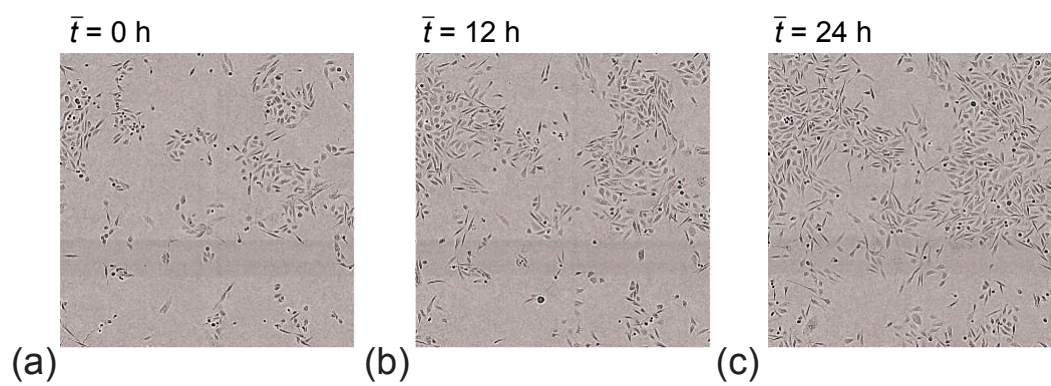


Fig. 1. ***In vitro* cell proliferation assay.** Population of PC-3 prostate cancer cells in a square field of view, of side length  $1440 \mu\text{m}$ . Images correspond to (a)  $\bar{t} = 0 \text{ h}$ , (b) 12 h, and (c) 24 h (Browning et al., 2018). Reproduced from Browning et al. (2018) with permission.

29 Mathematical models are often used to mimic cell biology experiments, and  
30 to quantify rates of cell proliferation (Cai et al., 2007; Jin et al., 2017; Nardini  
31 et al., 2016). One approach is to apply an individual-level, agent-based model  
32 (Frascoli et al., 2014). In this kind of model, agents represent individual cells,  
33 and these agents migrate and proliferate according to certain rules thought to  
34 be relevant to the application of interest (Treloar et al., 2014). Although agent-  
35 based models offer the capability to investigate individual-level details, most of  
36 these models adopt a conventional assumption that the rate of proliferation of  
37 individual cells in the population is taken to be a constant. This assumption,  
38 however, may not be applicable to real situations where the proliferation rate  
39 of individual cells in the population varies significantly.

40 The most commonly-used continuum model of cell proliferation is the clas-  
41 sical logistic growth model (Cai et al., 2007; Jin et al., 2016; Maini et al.,  
42 2004a; Maini et al., 2004b; Sengers et al., 2007; Sheardown and Cheng, 1996;  
43 Sherratt and Murray 1990; Vo et al., 2015). Although the classical logistic  
44 growth model is widely used to estimate the growth rate for populations of  
45 cells, there is an increasing awareness in the mathematical biology literature  
46 that cell populations do not always grow logistically (e.g. Gerlee, 2013; Powell  
47 et al., 2017; Sarapata and de Pillis 2014; Sewalt et al. 2016; West et al. 2001;  
48 Neufeld et al. 2017), and generalisations of the logistic growth model have been  
49 proposed (Jolicoeur and Pontier, 1989; Tsoularis and Wallace, 2002). Other  
50 types of models, where population growth is explicitly coupled to external  
51 factors, such as light availability (Pozzobon and Perré, 2018) and interactions  
52 with other populations (García-Algarra et al., 2014), have also been developed  
53 for specific biological applications. However, a limitation in each of these mod-  
54 elling frameworks is that the cell proliferation rate is treated as a constant,  
55 which amounts to neglecting heterogeneity.

56 In this work we consider a discrete modelling framework in which we deliber-  
57 ately introduce heterogeneity in the rates of migration and proliferation. The

58 continuum limit description of the discrete model leads to a complicated sys-  
59 tem of reaction-diffusion equations which simplifies to a generalisation of the  
60 classical logistic growth model when we apply the model to situations where  
61 there are, on average, no spatial variations in the agent density, such as the  
62 experimental image in Figure 1. We apply the extended logistic model to sim-  
63 ulate a proliferation assay using a distribution of heterogeneous proliferation  
64 rates that are estimated from the cell biology literature. Our results show that  
65 neglecting the role of heterogeneity can produce misleading results when the  
66 growth dynamics are interpreted in a standard way by simply calibrating the  
67 solution of the classical logistic growth model model to match the data. Un-  
68 like the classic logistic growth model, the extended model does not have an  
69 exact solution. To address this, we provide analytical insight into the role of  
70 heterogeneity by constructing approximate perturbation solutions in the limit  
71 of small variation in the proliferation rate.

72 Throughout this study we use a combination of dimensional and dimension-  
73 less parameters. Mathematical models, both discrete and continuum, are first  
74 presented using dimensional variables and dimensional parameters. All di-  
75 mensional quantities are indicated with an overbar. Later, when we apply the  
76 mathematical models to experimental data, and when we present some analy-  
77 sis of the mathematical models, we always work with dimensionless variables  
78 and parameters for which the overbar notation is dropped.

## 79 **2 Discrete model**

80 We motivate our work using a conceptually straightforward, lattice-based ex-  
81 clusion process on a hexagonal lattice. We apply this model to simulate *in*  
82 *vitro* cell proliferation assays, such as the experimental image in Figure 1. In  
83 our model, agents represent individual cells, and these agent are placed uni-  
84 formly, at a specified initial density, on a hexagonal lattice. We use a lattice of

85 size  $I \times J$  lattice sites, with lattice spacing  $\bar{\Delta}$ . Here,  $\bar{\Delta}$  can be thought of as a  
86 typical cell diameter, such as  $\bar{\Delta} = 20 \mu\text{m}$ . To simulate crowding effects, each  
87 lattice site can be occupied by, at most, one agent. Each lattice site is indexed,  
88  $\mathbf{s} = (i, j)$ , where  $i, j \in \mathbb{Z}^+$ , and each site is associated with a unique Cartesian  
89 coordinate (Jin et al., 2017). The total population of agents is composed of  
90  $N \geq 1$ , potentially distinct, subpopulations. Agents in each subpopulation are  
91 characterised by a potentially distinct migration probability per time step,  
92  $P_m^{(n)} \in [0, 1]$  for  $n = 1, 2, \dots, N$ . Furthermore, agents in each subpopulation  
93 are characterised by a potentially distinct proliferation probability per time  
94 step,  $P_p^{(n)} \in [0, 1]$  for  $n = 1, 2, \dots, N$ . The total number of agents at time  $t$  is  
95  $M(\bar{t})$ .

96 Cell migration and proliferation are modelled using a random sequential ran-  
97 dom update method (Treloar et al., 2014). To advance the discrete model from  
98 time  $\bar{t}$  to time  $\bar{t} + \bar{\tau}$ ,  $M(\bar{t})$  agents are selected at random, one at a time, with  
99 replacement. The selected agent attempts to move to one of the six nearest  
100 neighbour sites with probability  $P_m^{(n)}$ . The attempted migration event will be  
101 successful if the randomly chosen nearest neighbour target site is vacant. After  
102  $M(\bar{t})$  potential migration events have been attempted, another  $M(\bar{t})$  agents  
103 are selected at random, one at a time, with replacement. The selected agent  
104 will attempt to place a daughter agent on one of the six nearest neighbour sites  
105 with probability  $P_p^{(n)}$ . The attempted proliferation will only be successful if  
106 the randomly chosen nearest neighbour site is vacant. In the event that the po-  
107 tential proliferation event is successful, we make the simplest assumption that  
108 the daughter agent belongs to the same subpopulation as the mother agent.  
109 Once these potential motility and proliferation events have been attempted,  
110 we update  $M(\bar{t} + \bar{\tau})$ .

### 111 3 Continuum limit description

112 The continuum limit description of the discrete model can be derived us-  
 113 ing averaging arguments and mean field theory. We denote the probability  
 114 of finding an agent from subpopulation  $n$  at site  $\mathbf{s} = (i, j)$  as  $C_{\mathbf{s}}^{(n)} \in [0, 1]$ ,  
 115 for  $n = 1, 2, \dots, N$ . This probability can be thought of as corresponding to  
 116 averaging the occupancy of site  $\mathbf{s}$  over many identically prepared realisations  
 117 of the stochastic model. Therefore, the probability of site  $\mathbf{s}$  being vacant is  
 118  $\left(1 - \sum_{n=1}^N C_{\mathbf{s}}^{(n)}\right)$ . In the discrete model, migration events can act to either in-  
 119 crease or decrease the occupancy of site  $\mathbf{s}$ , whereas proliferation events can  
 120 only act to increase the occupancy of site  $\mathbf{s}$ . Accounting for these possibilities,  
 121 the change in average occupancy at site  $\mathbf{s}$  for agents from subpopulation  $n$ ,  
 122 from time  $\bar{t}$  to time  $\bar{t} + \bar{\tau}$  can be written as,

$$\begin{aligned}
 \delta C_{\mathbf{s}}^{(n)} = & \overbrace{\frac{P_m^{(n)}}{6} \left(1 - \sum_{n=1}^N C_{\mathbf{s}}^{(n)}\right) \sum_{\mathbf{s}' \in \mathcal{N}\{\mathbf{s}\}} C_{\mathbf{s}'}^{(n)}}^{\text{increase in occupancy due to migration into site } \mathbf{s}} \\
 & - \overbrace{\frac{P_m^{(n)}}{6} C_{\mathbf{s}}^{(n)} \sum_{\mathbf{s}' \in \mathcal{N}\{\mathbf{s}\}} \left(1 - \sum_{n=1}^N C_{\mathbf{s}'}^{(n)}\right)}^{\text{decrease in occupancy due to migration out of site } \mathbf{s}} \\
 & + \overbrace{\frac{P_p^{(n)}}{6} \left(1 - \sum_{n=1}^N C_{\mathbf{s}}^{(n)}\right) \sum_{\mathbf{s}' \in \mathcal{N}\{\mathbf{s}\}} C_{\mathbf{s}'}^{(n)}}^{\text{increase in occupancy due to proliferation into site } \mathbf{s}}, \quad (1)
 \end{aligned}$$

123 where  $\mathcal{N}\{\mathbf{s}\}$  denotes the set of six nearest-neighbour sites around site  $\mathbf{s}$ . In  
 124 Equation (1) we implicitly make the standard assumption that the average  
 125 occupancy of each lattice site is independent. This is the mean field assump-  
 126 tion. We expand each term in Equation (1) about site  $\mathbf{s}$  using Taylor series,  
 127 and neglect terms of  $\mathcal{O}(\bar{\Delta}^3)$ . Dividing both sides of the resulting expression by  
 128  $\bar{\tau}$ , and taking the limit as  $\bar{\Delta} \rightarrow 0$  and  $\bar{\tau} \rightarrow 0$  jointly, with  $\bar{\Delta}^2/\bar{\tau}$  held constant



129 we obtain,

$$\frac{\partial C_n(\bar{x}, \bar{y}, \bar{t})}{\partial \bar{t}} = \overbrace{\left( \frac{P_m^{(n)} \bar{\Delta}^2}{4\bar{\tau}} \right) \nabla \cdot \left[ (1 - S(\bar{x}, \bar{y}, \bar{t})) \nabla C_n(\bar{x}, \bar{y}, \bar{t}) + C_n(\bar{x}, \bar{y}, \bar{t}) \nabla S(\bar{x}, \bar{y}, \bar{t}) \right]}^{\text{unbiased motility mechanism with exclusion}} + \overbrace{\left( \frac{P_p^{(n)}}{\bar{\tau}} \right) C_n(\bar{x}, \bar{y}, \bar{t}) [1 - S(\bar{x}, \bar{y}, \bar{t})]}^{\text{unbiased proliferation mechanism with exclusion}}, \quad (2)$$

130 for  $n = 1, 2, \dots, N$ . The total population density is given by  $S(\bar{x}, \bar{y}, \bar{t}) = \sum_{n=1}^N C_n(\bar{x}, \bar{y}, \bar{t})$ .

131 In cell proliferation experiments, cells are placed uniformly on a two-dimensional  
132 substrate (Browning et al. 2018; Jin et al., 2017). Therefore, this kind of ini-  
133 tialisation means that there are, on average, no spatial gradients in cell density.

134 Under these conditions Equation (2) simplifies to

$$\frac{dC_n(\bar{t})}{d\bar{t}} = \bar{r}_n C_n(\bar{t}) [1 - S(\bar{t})], \quad (3)$$

135 where  $\bar{r}_n = P_p^{(n)} / \bar{\tau}$ , for  $n = 1, 2, 3, \dots, N$ . The total cell density  $S(\bar{t})$  then can  
136 be obtained by summing over the governing equations of  $N$  subpopulations to  
137 give,

$$\frac{dS(\bar{t})}{d\bar{t}} = \left( \sum_{n=1}^N \bar{r}_n C_n(\bar{t}) \right) [1 - S(\bar{t})]. \quad (4)$$

138 In this work we always deal with initial condition contains without any spa-  
139 tial gradients, which means that we are working with a system of ordinary  
140 differential equations (ODE) instead of a system of partial differential equa-  
141 tions (PDE). If we were to consider a different initial condition, such as a  
142 scratch assay or a barrier assay where there experiments are intentionally ini-  
143 tialised with some spatial gradients present, then we would have to work with  
144 Equation (2) instead of Equation (3).

145 Without loss of generality, when we apply Equation (3) we adopt the conven-

146 tion that  $\bar{r}_1 \geq \bar{r}_2 \geq \bar{r}_3 \geq \dots \geq \bar{r}_N$ , so that  $\bar{r}_1$  is the proliferation rate of the  
147 fastest-proliferating subpopulation,  $\bar{r}_2$  is the proliferation rate of the second  
148 fastest-proliferating subpopulation, and so on. We note that in the special case  
149 where we consider all the proliferation rates to be equal,  $\bar{r}_1 = \bar{r}_2 = \dots = \bar{r}_N$ ,  
150 we are dealing with a homogeneous population with a constant proliferation  
151 rate,  $\bar{\lambda}$ . The continuum limit description simplifies to,

$$\frac{dC(\bar{t})}{d\bar{t}} = \bar{\lambda}C(\bar{t})[1 - C(\bar{t})], \quad (5)$$

152 which is the classical logistic growth model (Murray, 2002), whose solution is  
153 given by,

$$C(\bar{t}) = \frac{C(0)}{[1 - C(0)]e^{-\bar{\lambda}\bar{t}} + C(0)}. \quad (6)$$

154 This exact solution is a sigmoid curve that monotonically increases from  $C(0)$ ,  
155 and approaches unity as  $\bar{t} \rightarrow \infty$ , provided that  $C(0) < 1$ . Since our system of  
156 ODEs, given by Equation (3), simplifies to the classical logistic model when all  
157 the proliferation rates are identical, we refer to Equation (3) as the *extended*  
158 *logistic growth model*.

159 To simplify our work we nondimensionalise time using the fastest proliferation  
160 rate,  $t = \bar{r}_1\bar{t}$ . Therefore Equation (3) becomes

$$\begin{aligned} \frac{dC_1(t)}{dt} &= C_1(t)[1 - S(t)], \\ \frac{dC_n(t)}{dt} &= r_n C_n(t)[1 - S(t)], \end{aligned} \quad (7)$$

161 where  $r_n = \bar{r}_n/\bar{r}_1$ , for  $n = 2, 3, \dots, N$ . Therefore, we now have a system of  
162 ODEs with non-dimensional proliferation rates of: unity,  $r_2, r_3, \dots, r_N$ , with  
163  $1 \geq r_2 \geq r_3 \geq \dots \geq r_N$ . This non-dimensionalisation allows us to compare  
164 the solutions of the model for different systems that are characterised by very  
165 different proliferation rates. In the non-dimensional format, Equation (4) be-

166 comes

$$\frac{dS(t)}{dt} = \left( C_1(t) + \sum_{n=2}^N r_n C_n(t) \right) [1 - S(t)]. \quad (8)$$

167 To be consistent, if we non-dimensionalise Equation (6) with  $t = \bar{\lambda}t$ , we obtain

$$C(t) = \frac{C(0)}{[1 - C(0)]e^{-t} + C(0)}. \quad (9)$$

168 Unlike the classical logistic model, Equation (7) does not have an exact so-  
169 lution. Therefore, we present numerical solutions that are obtained using a  
170 backward Euler approximation. In all cases we use a constant time step of  
171  $\delta t = 0.01$ , and Picard iteration with convergence tolerance  $\epsilon = 1 \times 10^{-5}$ .  
172 These choices of  $\delta t$  and  $\epsilon$  are sufficient to produce grid-independent numerical  
173 solutions of the model.

## 174 4 Results

### 175 4.1 Continuum-discrete match

176 All discrete results are presented in a non-dimensional format, on a lattice  
177 with unit lattice spacing and with time steps of unit duration,  $\Delta = \tau = 1$ .  
178 Note that  $\Delta$  and  $\tau$  can be re-scaled to correspond to any particular choices  
179 of dimensional  $\bar{\Delta}$  and  $\bar{\tau}$ . This means that we can re-scale any of these dimen-  
180 sionless simulations to correspond to a population of cells with arbitrary cell  
181 diameter, and arbitrary characteristic proliferation rate. Since we are focus-  
182 ing on the role of heterogeneity in cell proliferation, in all simulations we set  
183  $\Delta = P_m^{(n)} = 1$ , for  $n = 1, 2, \dots, N$ , and  $\tau = P_p^{(1)} = 0.01$ . In addition, we choose  
184  $I = 101$  and  $J = 117$ , so that the size of the simulation domain is  $100 \times 100$ .  
185 Periodic boundary conditions are applied to all simulations.

186 To explore the role of heterogeneity in population growth, we first consider  
187 simulations involving up to three subpopulations: subpopulation 1 has the  
188 fastest proliferation rate; subpopulation 2 has an intermediate proliferation  
189 rate; and subpopulation 3 has the slowest proliferation rate. We first perform  
190 three different types of discrete simulations initialised with different combina-  
191 tions of these three subpopulations. Each simulation is initialised so that the  
192 total number of agents occupies just 10% of the total number of lattice sites.  
193 In the first simulation we consider a homogeneous population that is com-  
194 posed entirely of agents from subpopulation 1,  $N = 1$ . The second simulation  
195 involves a heterogeneous population that is composed of equal proportions of  
196 agents from subpopulations 1 and 2,  $N = 2$ . The third simulation involves  
197 a heterogeneous population that is composed of equal proportions of agents  
198 from subpopulations 1, 2 and 3,  $N = 3$ . Snapshots from the discrete simu-  
199 lations are shown in Figure 2. A qualitative comparison of these snapshots  
200 shows that the growth dynamics are very different in the homogeneous and  
201 heterogeneous populations. Both the dynamics of the overall total population,  
202 and the dynamics of the various subpopulations depends on the details of the  
203 heterogeneity present in the system.

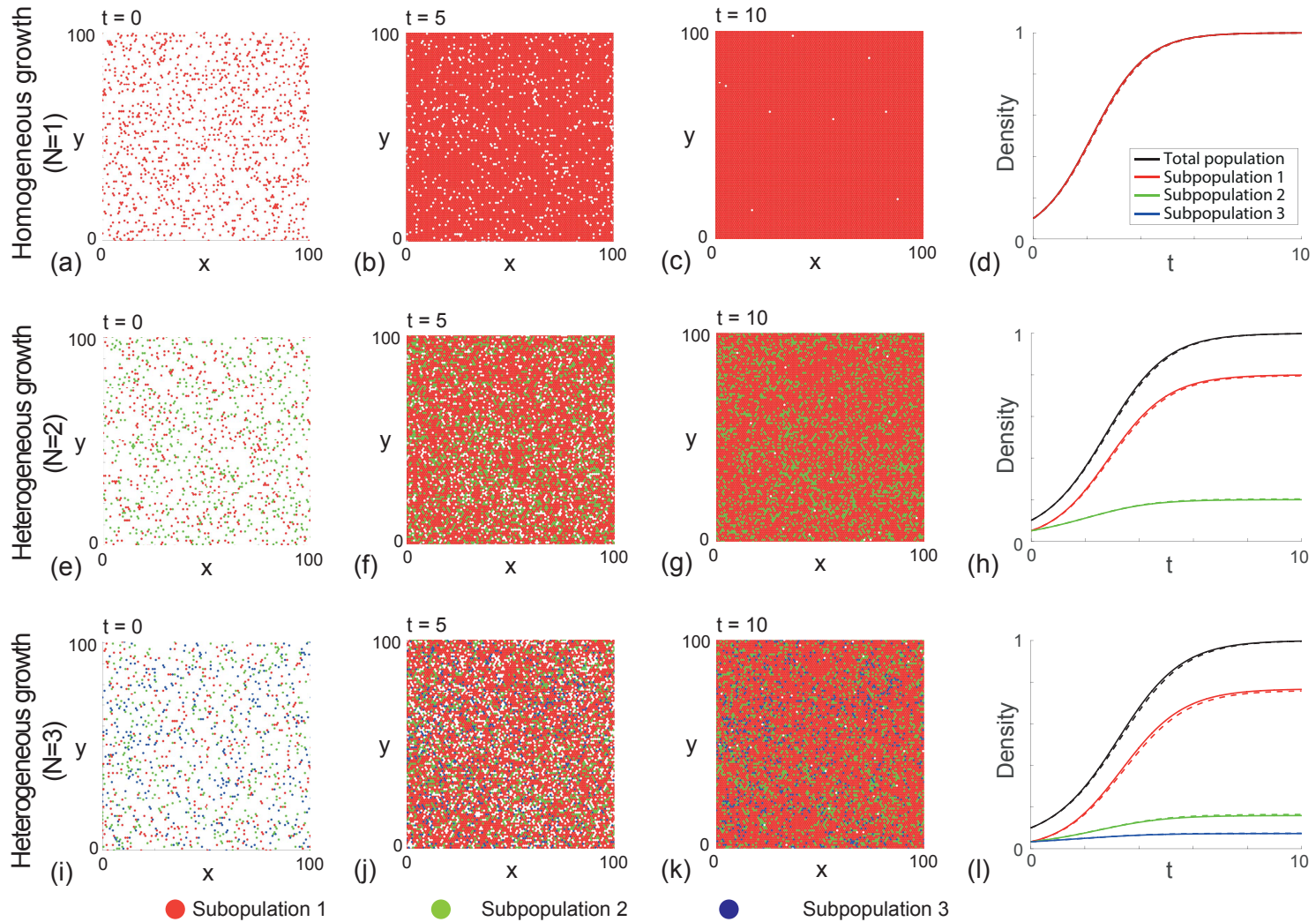


Fig. 2. **Discrete and continuum simulations of heterogeneous proliferation.** Snapshots are shown at  $t = 0, 5,$  and  $10$  for: (a)-(c) a homogeneous population,  $N = 1$ ; (e)-(g) a heterogeneous population,  $N = 2$ ; and (i)-(k) a heterogeneous population,  $N = 3$ . In each case, 10% of lattice sites are initially randomly occupied, with equal proportions of the various subpopulations. (d), (h), (l) show the corresponding continuum-discrete matches. The solid lines are solutions of the extended logistic model, dashed lines are averaged discrete results, obtained by considering 50 identically prepared realisations. In all plots red represents the fastest-proliferating subpopulation (subpopulation 1); green represents the intermediate subpopulation (subpopulation 2); and blue represents the slowest-proliferating subpopulation (subpopulation 3). All simulations correspond to  $P_p^{(1)} = 0.01$ ,  $P_p^{(2)} = 0.005$ ,  $P_p^{(3)} = 0.0025$ ,  $r_2 = 0.5$  and  $r_3 = 0.25$ .

204 To quantify the population growth, we plot the time evolution of the total  
205 averaged agent density, and superimpose the corresponding solution of Equa-  
206 tion (7). For the homogeneous population in Figure 2(d), the continuum limit  
207 simplifies to the classical logistic growth model, while for the heterogeneous  
208 populations in Figure 2(h) and (l), the extended logistic model applies. Over-  
209 all we see that the quality of the match between the solution of the continuum  
210 model and averaged data from the discrete simulations is excellent. Therefore,  
211 this comparison indicates that the continuum limit description is a useful and  
212 accurate mathematical tool that can be used to study the proliferation of het-  
213 erogeneous populations without relying on repeated stochastic simulations.

#### 214 *4.2 Comparison of the classical logistic growth model and the extended logistic* 215 *model*

216 As mentioned in the Introduction, although the classical logistic growth model  
217 is widely used when interpreting data from cell biology experiments (Cai et  
218 al., 2007; Jin et al., 2016; Maini et al., 2004a; Maini et al., 2004b; Sengers et  
219 al., 2007; Sheardown and Cheng, 1996; Sherratt and Murray 1990; Vo et al.,  
220 2015), this standard approach neglects any heterogeneity in cell proliferation  
221 rate. To provide insight into how well the classical logistic growth model is  
222 able to predict and describe the growth of heterogeneous populations, we now  
223 calibrate the solution of the classical logistic growth model in an attempt to  
224 match the solution of the extended logistic model which explicitly accounts  
225 for heterogeneous growth.

226 We consider two different initial conditions for a population that is composed  
227 of three different subpopulations,  $N = 3$ . Again, we refer to these subpopula-  
228 tions as subpopulations 1, 2, and 3. For both initial conditions we consider, we  
229 distribute the total population uniformly across the domain so that the ini-  
230 tial total density is 10% of the carrying capacity density. In the first case we

231 choose the initial condition so that the total population is initially composed  
232 of 75% of agents from subpopulation 1, 20% of agents from subpopulation  
233 2, and 5% of agents from subpopulation 3, as shown in Figure 3(a). In the  
234 second case we choose the initial condition so that the total population is  
235 initially composed of 5% of agents from subpopulation 1, 20% of agents from  
236 subpopulation 2, and 75% of agents from subpopulation 3, as shown in Figure  
237 3(b). These choices of initial condition mean that the first case is composed of  
238 a small proportion of relatively quiescent agents (di Fagagna et al., 2003), and  
239 the second case corresponds to a population that contains a small proportion  
240 of rapidly proliferating agents, such as is thought to be relevant to cancer  
241 progression (Davis et al., 2017). The solution of the extended logistic growth  
242 model for these two scenarios of heterogeneous growth are shown in Figure  
243 3(b) and (d), respectively.

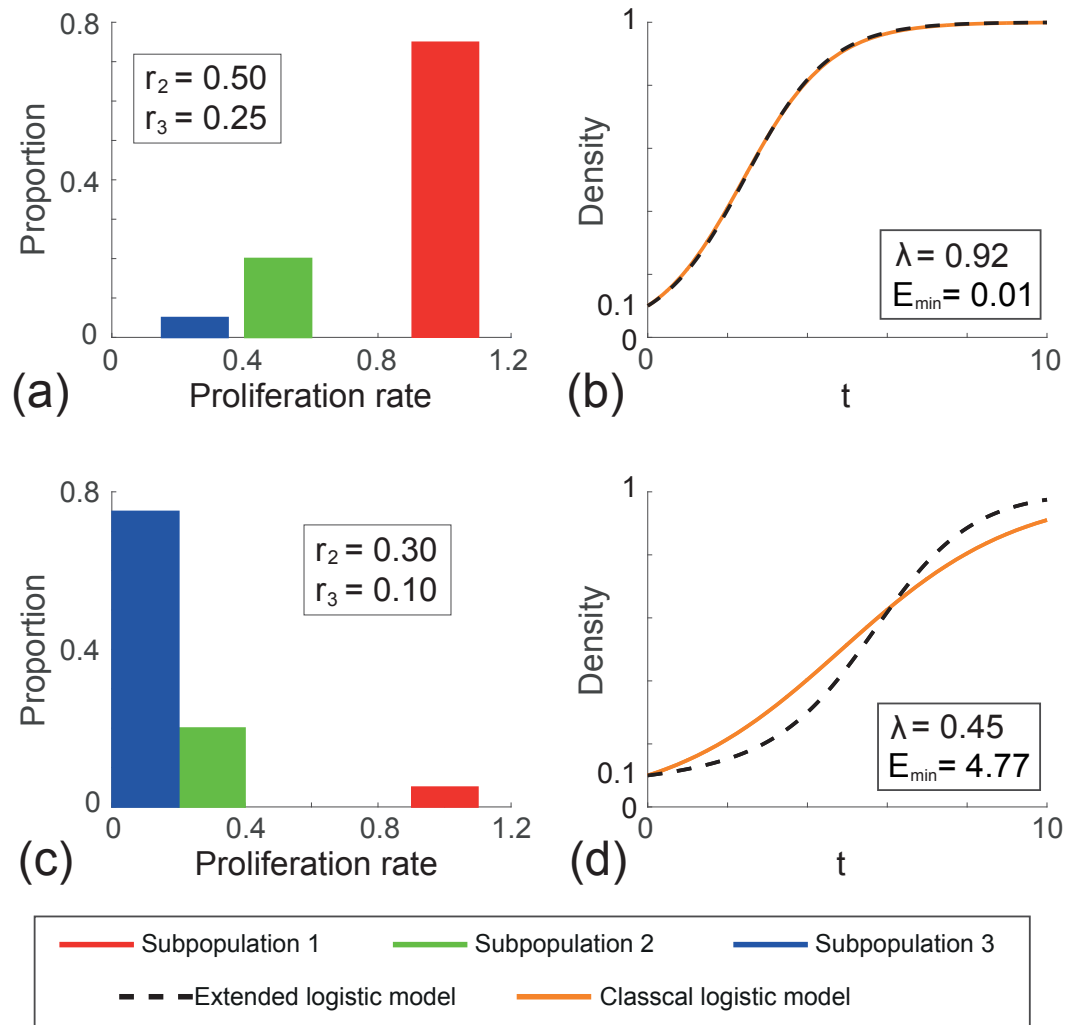


Fig. 3. **Comparison of the classical logistic growth model to the extended model for heterogeneous growth.** (a) and (c) Initial distribution of proliferation rate for the two heterogeneous populations. In all cases, red represents the fastest-proliferating subpopulation (subpopulation 1); green represents the intermediate subpopulation (subpopulation 2); and blue represents the slowest-proliferating subpopulation (subpopulation 3). In each case, the time evolution of the total density from the extended model, together with the best-fit classical logistic growth curve, is plotted in (b) and (d).



244 Again, we recall that standard approaches to interpreting cell proliferation  
245 assays is to calibrate the solution of the classical logistic growth model to  
246 match the experimental data, and to provide an estimate of the proliferation  
247 rate (Cai et al., 2007; Jin et al., 2016; Maini et al., 2004a; Maini et al., 2004b;  
248 Sengers et al., 2007; Sheardown and Cheng, 1996; Sherratt and Murray 1990;  
249 Vo et al., 2015). This standard approach implicitly neglects the role of het-  
250 erogeneity, so it is of interest for us to take the population growth curves for  
251 these heterogeneous populations in Figure 3(b) and (d), and to calibrate the  
252 solution of the classical logistic growth model to match this data. We calibrate  
253 the solution of the classical logistic growth model to the density data in Figure  
254 3(b) and (d) using MATLAB's *lsqcurvefit* function, and show the best match  
255 in Figure 3(b) and (d). This calibration provides an estimate of  $\lambda$  that is as-  
256 sociated with the best fit of the standard model to the total density data. We  
257 are also interested in understanding the quality of match between the best fit  
258 solution of the classical logistic growth model and the heterogeneous density  
259 data. To quantify the quality of match we use a least-squares measure,

$$E = \sum_{l=1}^{1000} [C(t_l) - S(t_l)]^2, \quad (10)$$

260 where  $C(t)$  is the best fit solution of the classical logistic growth model, and  
261  $S(t)$  is the total density associated with the extended logistic growth model.  
262 Here we measure  $E$  in the interval  $0 \leq t \leq 10$ , by evaluating both  $C(t)$  and  
263  $S(t)$  at 1000 equally-spaced time points,  $t_l$  for  $t_l = 0, 0.01, 0.02, \dots, 10$ .

264 A simple visual comparison of the best fit classical logistic growth model and  
265 the solution of the extended model in Figure 3(b) shows that the standard  
266 approach of neglecting heterogeneity leads to an excellent match. However, re-  
267 sults in Figure 3(d) indicate that the best fit classical logistic model matches  
268 the heterogeneous growth curve poorly. This qualitative assessment of the  
269 quality of match is confirmed quantitatively by our estimates of  $E$ , as re-  
270 ported in Figure 3. Overall, we see that the standard approach of neglecting

271 heterogeneity can sometimes lead to reasonable outcomes, whereas in other  
272 cases the neglect of heterogeneity is unsatisfactory. We anticipate that the ini-  
273 tial distribution of proliferation rates across the initial subpopulations plays  
274 an important role in determining the suitability of this standard approach.  
275 We now investigate this question further by applying our extended model to  
276 some data from the literature

## 277 5 Case study

278 We will now compare the performance of the classical logistic growth model  
279 and the extended logistic growth model by simulating proliferation assays in  
280 which the distributions of heterogeneous proliferation rates are taken from  
281 recent experimental measurements. In particular, we work with data from two  
282 human melanoma cell lines (Haass et al., 2014): (i) the 1205Lu cell line, which  
283 we refer to as cell line 1, and (ii) the WM983C cell line, which we refer to as cell  
284 line 2. The data we use to characterize the distribution of proliferation rates  
285 comes directly from Haass et al. (2014) where they use a specialised fluorescent  
286 technique to characterise the cell cycle of individual melanoma cells. Data from  
287 Haass et al. (2014) reports the duration of time spent in the S/G2/M phase of  
288 the cell cycle for groups of at least 20 individual cells from multiple melanoma  
289 cell lines. Since the S/G2/M cell cycle phase is closely related to the process  
290 of cell division, we treat the heterogeneity in these measurements as being  
291 representative of the heterogeneity present in the entire cell cycle.

292 Haass' data reports the duration of time that at least 20 individual cells spend  
293 in the S/G2/M cell cycle phase (Haass et al., 2014). We group these individual  
294 measurements of duration into three subgroups. We choose the subgroups so  
295 that each column in the histogram of this data has approximately the same  
296 width, as shown in Figure 4(a)-(b). Since Haass' data is reported in terms of a  
297 duration of time spent in the cell cycle, we convert these durations into rates

298 by dividing  $\log_e(2)$  by the reported durations. Here, the  $\log_e(2)$  term comes  
299 from making the simple assumption that cells are growing exponentially. The  
300 details of the raw experimental data are given in the Supplementary Material  
301 document. Presenting the dimensional rates in Figure 4(c)-(d) indicates that  
302 the distribution of proliferation rate in cell line 1 is approximately symmetric,  
303 whereas the distribution of rates for cell line 2 is positively skewed.

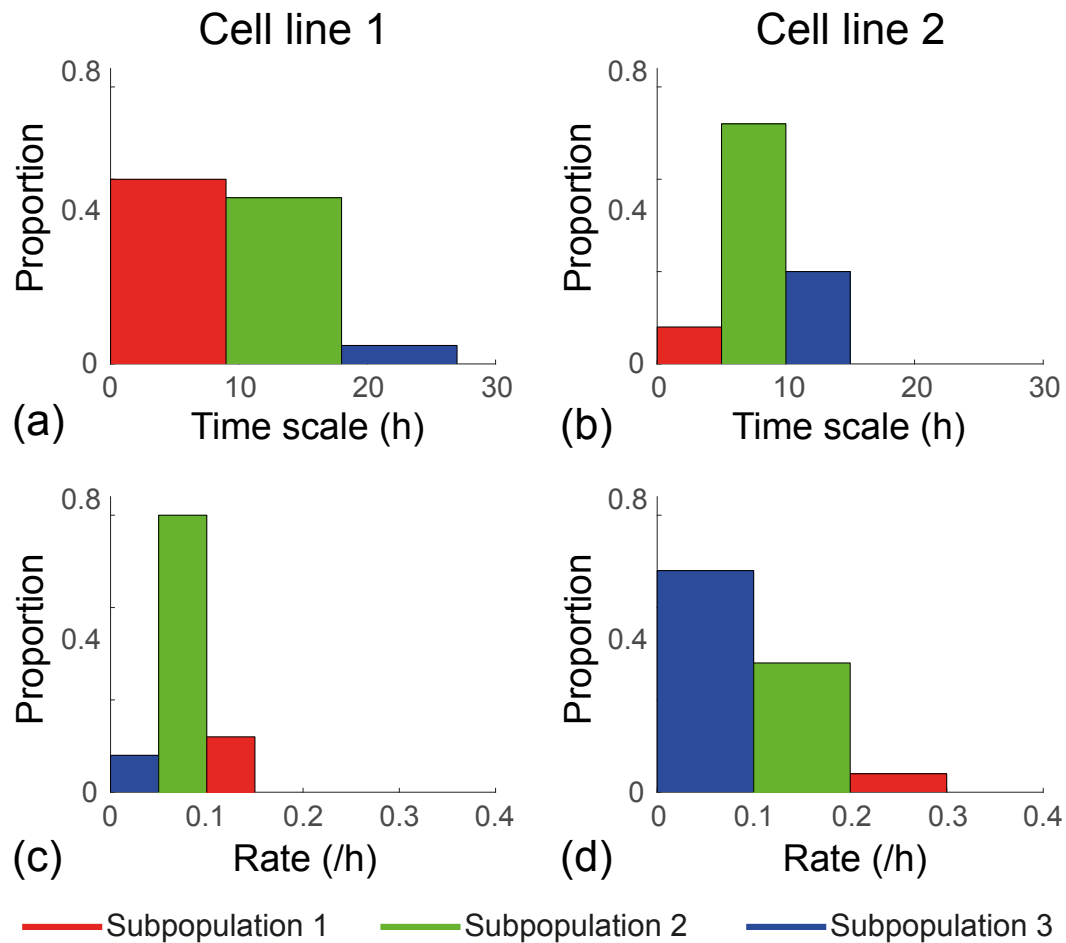


Fig. 4. **Experimental data from Haass et al. (2014).** (a)-(b) Histograms showing the distribution of the time scale associated with the S/G2/M cell cycle for cell lines 1 and 2, respectively. (c)-(d) Histograms showing the distribution of rates associates with the S/G2/M cell cycle for cell lines 1 and 2, respectively. The time scales are converted to rates by dividing  $\log_e(2)$  by the time scale. For both cell lines: red indicates the fastest-proliferating subpopulation (subpopulation 1); green indicates the intermediate subpopulation (subpopulation 2); and blue indicates the slowest-proliferating subpopulation (subpopulation 3).

304 To apply our models using the heterogeneous proliferation rate data in Fig-  
305 ure 4, we non-dimensionalise the proliferation rate data by dividing each rate  
306 by the fastest-proliferation rate for each cell line. This data, presented as  
307 histograms in Figure 5(a)-(e), shows the distribution of non-dimensional pro-  
308 liferation rates for both cell lines. We now use these histograms to specify  
309 both the initial proliferation rates, and the initial distribution of the three  
310 subpopulations in the discrete model and the corresponding extended logistic  
311 continuum model.

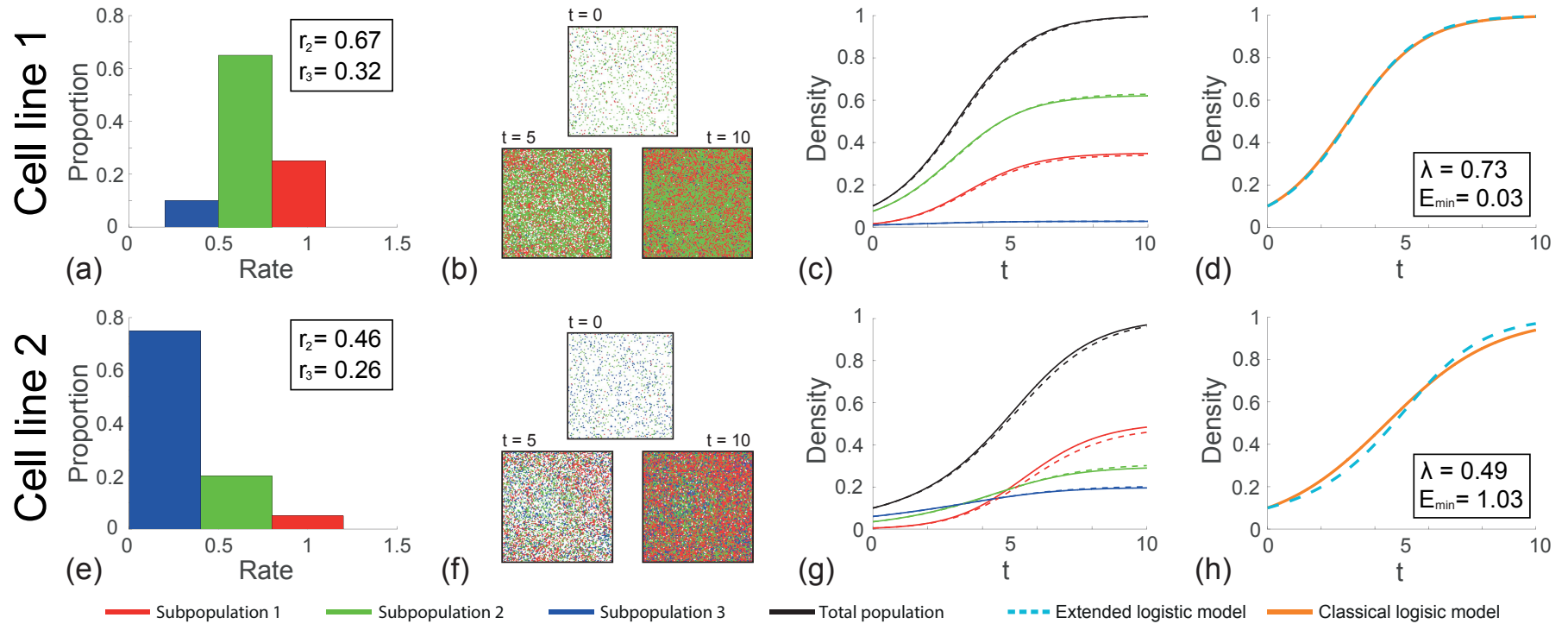


Fig. 5. **Comparison of the classical logistic growth model to the extended model for experimental cell lines 1 and 2.** (a) and (e) Initial distribution of proliferation rate for cell lines 1 and 2, respectively. (b) and (f) Snapshots of simulations at  $t = 0, 5,$  and  $10$  for both experimental cell lines. (c) and (g) The continuum-discrete match of the time evolution of the densities for experimental cell lines 1 and 2, respectively. Solid lines represent the numerical solutions of the extended model, and the dashed lines represent the averaged simulation data over 50 identically prepared realisations. (d) and (h) Calibrated solution of the classical logistic growth model superimposed with the total density profile computed using the extended model. For both of experimental cell lines, red represents the fastest-proliferating subpopulation (subpopulation 1); green represents the intermediate subpopulation (subpopulation 2); and blue represents the slowest-proliferating subpopulation (subpopulation 3). For cell line 1,  $P_p^{(1)} = 0.01$ ,  $P_p^{(2)} = 0.0067$ , and  $P_p^{(3)} = 0.0032$ . For cell line 2,  $P_p^{(1)} = 0.01$ ,  $P_p^{(2)} = 0.0046$ , and  $P_p^{(3)} = 0.0026$ .

312 We first model the heterogeneous population growth for cell line 1 and 2 using  
313 the discrete model. For each cell line, agents are initially distributed uniformly  
314 on the lattice so that 10% of lattice sites are occupied. We are also careful to  
315 ensure that the initial proportions of subpopulation 1, 2 and 3 correspond to  
316 the proportions of the three subpopulations in the histograms in Figure 5(a)  
317 and (e). Snapshots of the growing cell populations for both cell lines are given  
318 in Figure 5(b) and (f). These snapshots immediately reveal some interesting  
319 features. For cell line 1, the distribution of the three subpopulations remains  
320 similar over time, as there appears to be roughly equal proportions of red,  
321 green and blue agents at  $t = 10$  as there are initially, at  $t = 0$ . However, we  
322 observe very different behaviour for cell line 2, as the relative abundance of the  
323 three subpopulations changes dramatically over time. For example, at  $t = 0$ ,  
324 we see that subpopulation 1 is the least abundant subpopulation. However,  
325 by the end of the growth process, at  $t = 10$ , subpopulation 1 is the most  
326 abundant subpopulation. These qualitative trends are also clear in Figure 5(c)  
327 and (g) where we compare averaged discrete data from repeated simulations of  
328 the stochastic model and the solution of the corresponding continuum model.  
329 In addition to quantifying the behaviour we see in the discrete snapshots,  
330 the solution of the continuum model in Figure 5(c) and (g) confirm that the  
331 continuum model is an accurate approximation of the discrete model.

332 To examine the implications of taking a standard approach and neglecting  
333 the role of heterogeneity, we also calibrate the solution of the classical logistic  
334 model to the total density data in Figure 5(c) and (g). Following the same  
335 approach described in Section 4.2, results in Figure 5(d) and (h) show the evo-  
336 lution of the total cell density profile superimposed with the best-fit classical  
337 logistic growth curves for cell line 1 and 2, respectively. Interestingly, the qual-  
338 ity of match between the classical logistic growth model and the heterogenous  
339 population growth curve is relatively good for cell line 1, whereas the quality  
340 of match for cell line 2 is poor.

341 These results show that the consequences of neglecting the role of hetero-  
342 geneity is subtle. In particular, under some circumstances it is possible to  
343 accurately predict the growth of a heterogeneous cell population using the  
344 classical logistic growth model, whereas in other circumstances the classical  
345 logistic growth model provides a poor match.

## 346 **6 Analytical insight for two subpopulations ( $N = 2$ )**

347 To support our numerical solutions of the continuum model developed in Sec-  
348 tion 3, we now provide some simple analysis. For brevity we concentrate on  
349 the case in which there are two subpopulations present, with densities  $C_1(t)$   
350 and  $C_2(t)$ . In this case the extended model, Equation (7), simplifies to

$$\begin{aligned}\frac{dC_1(t)}{dt} &= C_1(t)[1 - S(t)], \\ \frac{dC_2(t)}{dt} &= r_2 C_2(t)[1 - S(t)],\end{aligned}\tag{11}$$

351 where  $r_2 \leq 1$ . The governing equation for the evolution of the total density is

$$\frac{dS(t)}{dt} = [C_1(t) + r_2 C_2(t)][1 - S(t)].\tag{12}$$

352 The solutions for both  $C_1(t)$  and  $C_2(t)$  are sigmoid curves that monotonically  
353 increase from the initial densities,  $C_1(0)$  and  $C_2(0)$ , provided that  $C_1(0) +$   
354  $C_2(0) < 1$ . In the long time limit the solution of Equation (11) reaches a  
355 steady state solution, where  $S(t) \rightarrow 1$  as  $t \rightarrow \infty$ . To analyse this long time  
356 behaviour we denote the steady state densities as,

$$\mathcal{C}_1 = \lim_{t \rightarrow \infty} C_1(t), \quad \mathcal{C}_2 = \lim_{t \rightarrow \infty} C_2(t),\tag{13}$$

357 so that we have  $\mathcal{C}_1 + \mathcal{C}_2 = 1$ .



358 *6.1 Exact steady state concentrations*

359 It is not immediately clear what the steady state values  $\mathcal{C}_1$  and  $\mathcal{C}_2$  are from  
360 Equation (11), without first solving the transient model for the long time  
361 behaviour (Simpson et al., 2007). Furthermore, it is unclear how these steady  
362 state densities depend on the initial condition,  $C_1(0)$  and  $C_2(0)$ , or on the  
363 proliferation rate  $r_2$ . To provide insight into this question, we can solve for  
364  $\mathcal{C}_1$  and  $\mathcal{C}_2$  directly by first dividing one of the equations in (11) by the other,  
365 separating variables, and integrating to give

$$C_2(t) = \frac{C_2(0)}{[C_1(0)]^{r_2}} [C_1(t)]^{r_2}. \quad (14)$$

366 This relationship holds for all  $t$ . By substituting Equation (14) into Equation  
367 (11), we eliminate  $C_2(t)$  to give

$$\frac{dC_1(t)}{dt} = r_1 C_1(t) \left( 1 - C_1(t) - \frac{C_2(0)}{[C_1(0)]^{r_2}} [C_1(t)]^{r_2} \right). \quad (15)$$

368 This equation is now a direct analogue of the classical logistic growth model.  
369 For general values of  $r_2 < 1$ , Equation (15) has no exact solution. However,  
370 in this form it is easy to read off the steady-state value by setting the time  
371 derivative to zero, resulting in

$$1 - \mathcal{C}_1 - \frac{C_2(0)}{[C_1(0)]^{r_2}} (\mathcal{C}_1)^{r_2} = 0. \quad (16)$$

372 Equation (16) is a simple algebraic equation which can be solved using any  
373 iterative numerical method, such as MATLAB's *fsolve* function. The value of  
374  $\mathcal{C}_2$  is then given by  $\mathcal{C}_2 = 1 - \mathcal{C}_1$ .

375 Results in Figure 6(a)-(b) show two examples where we have used this ap-  
376 proach to directly calculate  $\mathcal{C}_1$  and  $\mathcal{C}_2$ . These predictions are superimposed on

377 the associated transient solutions of Equation (11), showing that the direct  
378 method provides a simple and accurate way to calculate the long-time steady  
379 solution, without needing to use numerical integration to evaluate the long  
380 time limit of the transient solution.

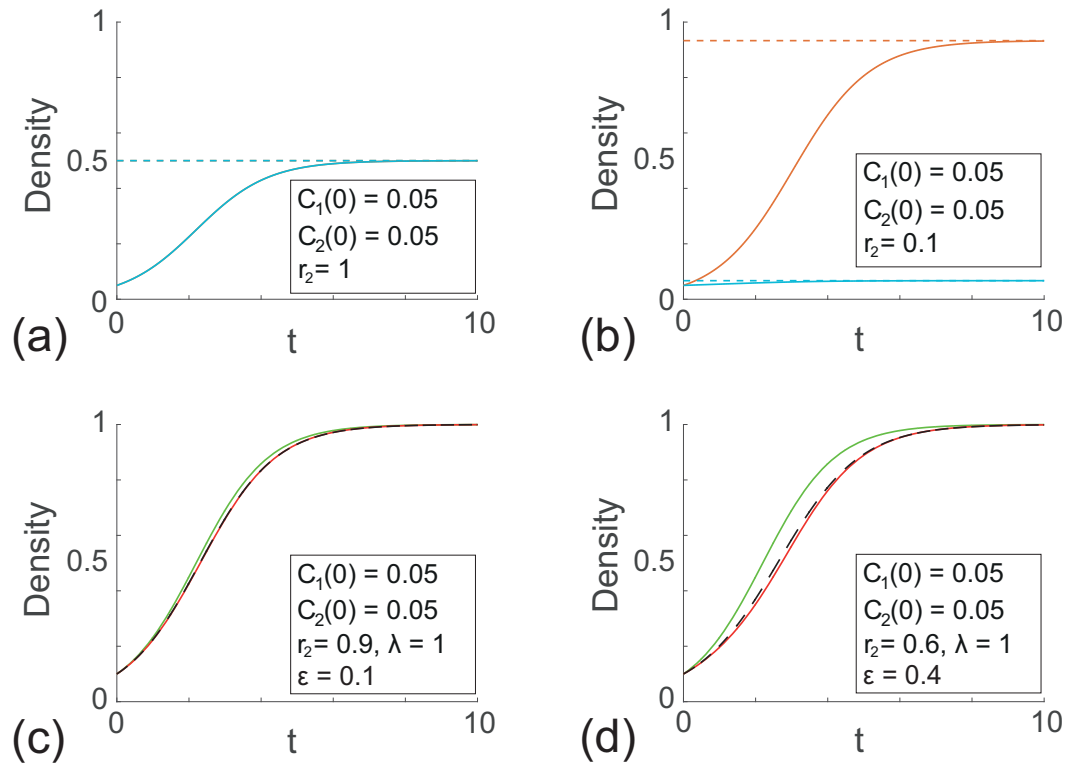


Fig. 6. **Analytical insight into the extended logistic model with two subpopulations**,  $N = 2$ . (a)-(b) Steady state results (dashed) compared to the full transient numerical solutions (solid). Here, the first subpopulation is shown in orange, and the second subpopulation is shown in blue. (c)-(d) Comparison of the transient numerical solutions of total density (black) with the two-term perturbation solutions in the limit of small heterogeneity. The  $\mathcal{O}(1)$  perturbation solution is plotted in green and the two-term  $\mathcal{O}(\varepsilon)$  perturbation solution is plotted in red.

381 *6.2 Approximate results for small heterogeneity*

382 Although the extended logistic growth model given by Equation (11) does not  
383 have an exact solution, we can obtain approximate results for in the limit of  
384 small heterogeneity. To explore this we consider  $r_2 = 1 - \varepsilon$ , where  $\varepsilon \ll 1$ , and  
385 propose the perturbation solution (Murray, 2012)

$$\begin{aligned} C_1(t) &= C_1^{(0)}(t) + \varepsilon C_1^{(1)}(t) + \mathcal{O}(\varepsilon^2), \\ C_2(t) &= C_2^{(0)}(t) + \varepsilon C_2^{(1)}(t) + \mathcal{O}(\varepsilon^2), \end{aligned} \quad (17)$$

386 where the superscripts (0) and (1) represent the leading order and first cor-  
387 rection terms, respectively. The asymptotic solution for the total population  
388 is obtained by summing over the solutions for the two subpopulations:

$$S(t) = S^{(0)}(t) + \varepsilon S^{(1)}(t) + \mathcal{O}(\varepsilon^2). \quad (18)$$

389 Substituting Equation (17) into the extended logistic model, given by Equation  
390 (11), gives the system

$$\begin{aligned} \frac{dC_1^{(0)}(t)}{dt} &= C_1^{(0)}(t) [1 - S^{(0)}(t)], \\ \frac{dC_2^{(0)}(t)}{dt} &= C_2^{(0)}(t) [1 - S^{(0)}(t)], \end{aligned} \quad (19)$$

391 with  $C_1^{(0)}(0) = C_1(0)$ ,  $C_2^{(0)}(0) = C_2(0)$ . Correspondingly, the  $\mathcal{O}(1)$  equation  
392 for the total population is

$$\frac{dS^{(0)}(t)}{dt} = S^{(0)}(t) [1 - S^{(0)}(t)], \quad (20)$$

393 with  $S^{(0)}(0) = S(0)$ . Equation (20) is the standard logistic growth model with

394 the explicit solution (Murray, 2002)

$$S^{(0)}(t) = \frac{S(0)}{[1 - S(0)]e^{-t} + S(0)}. \quad (21)$$

395 This is to be expected since our leading order problem holds for  $\epsilon = 0$ , in  
 396 which case both populations have the same proliferation rate, so effectively  
 397 there is one population. Solving for the individual subpopulations gives the  
 398 leading order solutions

$$\begin{aligned} C_1^{(0)}(t) &= \frac{C_1(0)}{[1 - S(0)]e^{-t} + S(0)}, \\ C_2^{(0)}(t) &= \frac{C_2(0)}{[1 - S(0)]e^{-t} + S(0)}. \end{aligned} \quad (22)$$

399 For  $\epsilon \ll 1$ , we proceed to solve for the correction terms. The governing equa-  
 400 tions for the individual populations are

$$\begin{aligned} \frac{dC_1^{(1)}(t)}{dt} &= C_1^{(1)}(t)[1 - S^{(0)}(t)] - C_1^{(0)}(t)S^{(1)}(t), \\ \frac{dC_2^{(1)}(t)}{dt} &= [C_2^{(1)}(t) - C_2^{(0)}(t)][1 - S^{(0)}(t)] - C_2^{(0)}(t)S^{(1)}(t), \end{aligned} \quad (23)$$

401 while the corresponding equation for the total density is

$$\frac{dS^{(1)}(t)}{dt} = S^{(1)}(t)[1 - 2S^{(0)}(t)] - C_2^{(0)}(t)[1 - S^{(0)}(t)]. \quad (24)$$

402 Equation (24) has an explicit solution

$$S^{(1)}(t) = \frac{C_2(0)[S(0) - 1]te^{-t}}{\{-e^{-t}[1 - S(0)] - S(0)\}^2}. \quad (25)$$

403 Neglecting higher order terms we obtain the two-term perturbation solution

404 for the total density

$$S(t) = \frac{S(0)}{[1 - S(0)]e^{-t} + S(0)} + \varepsilon \frac{C_2(0)[S(0) - 1]te^{-t}}{\{-e^{-t}[1 - S(0)] - S(0)\}^2} + \mathcal{O}(\varepsilon^2). \quad (26)$$

405 To demonstrate the effectiveness of this approximation, the  $\mathcal{O}(1)$  and  $\mathcal{O}(\varepsilon)$   
406 perturbation solutions for the total density are plotted in Figure 6(c) and (d).  
407 The corresponding full numerical solution is also presented. For a moderately  
408 small amount of heterogeneity in the population ( $\varepsilon = 0.1$ , Figure 6(c)), the  
409 leading order term (solid green) provides a reasonably good approximation  
410 of the numerical solution (dashed black). However, for larger heterogeneity  
411 ( $\varepsilon = 0.4$ , Figure 6(d)), we see that the leading order term is no longer close  
412 to the numerical solution, and instead the full two-term perturbation solution  
413 Equation (26) (solid red) is required to provide a good approximation. These  
414 plots provide further evidence that when the population is almost homogenous,  
415 then the classical logistic model provides a good approximation. However, as  
416 heterogeneity becomes more pronounced, then our extended logistic growth  
417 model does a much better job at describing the dynamics. Furthermore, pro-  
418 vided the heterogeneity is not too great, our two-term perturbation solution  
419 acts as a very good analytical approximation.

## 420 7 Conclusions

421 In this study we develop discrete and continuum models of cell migration and  
422 cell proliferation that allow us to explicitly investigate the role of heterogeneity,  
423 with a particular emphasis on the role of heterogeneity in the proliferation rate.  
424 Despite the fact that heterogeneity is commonly observed in cell populations,  
425 and is thought to play an important role in disease progression and tissue  
426 repair (Evan and Vousden, 2001; Haridas et al., 2017; Pavlath et al., 1998),

427 standard mathematical models of cell migration and cell proliferation neglect  
428 to account for heterogeneity. Indeed, most standard mathematical models of  
429 cell proliferation simply treat the proliferation rate as a constant.

430 To explore the role of heterogeneity, we start by developing a discrete mod-  
431 elling framework to simulate cell migration and cell proliferation, modulated  
432 by crowding effects. The key point of the model is to deliberately introduce  
433 heterogeneity in the individuals within the population. The continuum limit  
434 description of the discrete model leads to a system of coupled, nonlinear ODEs.  
435 It is of interest to note that in the simplest case where the proliferation rates  
436 of each subpopulation are identical, the system of ODEs simplifies to the clas-  
437 sical logistic growth model. Therefore, we call the new model the extended  
438 logistic growth model. Averaged data obtained from repeated simulations of  
439 the discrete model compare very well with the solution of the extended logistic  
440 growth model.

441 To explore the consequences of taking a standard approach and neglecting  
442 the role of heterogeneity, we perform a set of *in silico* experiments and gen-  
443 erate density profiles describing the growth of a heterogeneous population of  
444 cells. We calibrate the solution of the classical logistic equation to match that  
445 data. Interestingly, while the classical logistic growth model can provide an  
446 accurate prediction of the growth of some kinds of heterogeneous populations,  
447 we also find that in some circumstances the classical approach can not make  
448 accurate predictions. We also generate *in silico* data by parameterising the  
449 extended logistic growth model with a set of heterogeneous proliferation rates  
450 from recent experimental measurements. Again, we find that the classical lo-  
451 gistic model performs very well under some conditions, but it performs poorly  
452 for others. Overall, we find that when the heterogeneous population contains  
453 a small proportion of relatively fast proliferating cells, the classical logistic  
454 equation performs poorly. Therefore, we suggest that care ought to be ex-  
455 ercised when modelling the growth of certain cell populations. For example,

456 when modelling a population of cells that might involve mutations that act  
457 to increase the proliferation rate in a small subpopulation (e.g. Davis et al.,  
458 2017), the extended logistic growth model might be more accurate than the  
459 classical logistic equation.

460 Unlike the classical logistic equation, the extended logistic growth model does  
461 not have an exact solution. Therefore, in general, we have to rely on numeri-  
462 cal solutions. However, we also show how to provide some further insight by  
463 obtaining analytical solutions in the case where there are just two subpopu-  
464 lations present,  $N = 2$ . We obtain exact expressions for the long-time steady  
465 state solution, and show that these exact expressions can be solved numeri-  
466 cally to predict the steady state solution without using numerical integration  
467 to solve the full transient model. Furthermore, we also obtain approximate  
468 insight by constructing perturbation solutions in the limit that the degree  
469 of heterogeneity is small. The perturbation solutions are insightful since the  
470  $\mathcal{O}(1)$  perturbation solution for the total cell density is the classical logistic  
471 equation. The  $\mathcal{O}(\varepsilon)$  perturbation solution provides a correction term that is  
472 accurate even when we consider a relatively modest degree of heterogeneity in  
473 the system.

474 Although we have focused here on the question of developing mathematical  
475 tools and mathematical insight into the role of heterogeneity in population  
476 dynamics associated with populations of cells, it seems likely that the ideas  
477 explored here will have consequences beyond the cell biology literature. For  
478 example, classical logistic models, with constant growth rates, are also com-  
479 monly used in mathematical ecology (e.g. Chan and Kim, 2013), and there is  
480 also an awareness in the ecology literature that ecological populations do not  
481 always grow logistically (e.g. Taylor and Hastings, 2005). Therefore, perhaps  
482 some of the ideas developed here might also play a role in our understanding of  
483 ecological population dynamics. Another feature of our work is that we have  
484 focused exclusively on heterogeneity in cell proliferation rates. However, we



485 note that there is also considerable interest in developing quantitative, predic-  
486 tive mathematical models which incorporate heterogeneity in cell migration  
487 (e.g. Read et al., 2016). Again, it seems likely that the kind of approach taken  
488 here would also be of interest in the context of exploring heterogeneity in cell  
489 migration. These open questions could be considered in future studies.

490 *Acknowledgments.* This work is supported by the Australian Research Council  
491 (DP140100249, DP170100474).

492 **References**

- 493 [1] F.Q. An, M. Matsuda, H. Fujii, R.F. Tang, H. Amemiya, Y.M. Dai, Y.  
494 Matsumoto. Tumor heterogeneity in small hepatocellular carcinoma: Analysis  
495 of tumor cell proliferation, expression and mutation of p53 and  $\beta$ -catenin.  
496 *International Journal of Cancer*. 93 (2001) 468–474.
- 497 [2] J. Arino, L. Wang, G.S. Wolkowicz. An alternative formulation for a delayed  
498 logistic equation. *Journal of Theoretical Biology*. 241 (2006) 109–119.
- 499 [3] B. Azzarone, A. Macieira-Coelho. Heterogeneity of the kinetics of proliferation  
500 within human skin fibroblastic cell populations. *Journal of Cell Science*. 57 (1982)  
501 177–187.
- 502 [4] B.T. Bajar, A.J. Lam, R.K. Badiie, Y.-H. Oh, J. Chu, X.X. Zhou, N. Kim, B.B.  
503 Kim, M. Chung, A.L. Yablonovitch, B.F. Cruz, K.Kulalert, J.J. Tao, T. Meyer,  
504 X.-D. Su, and M.Z. Lin. Fluorescent indicators for simultaneous reporting of all  
505 four cell cycle phases. *Nature Methods* 13 (2016) 993–996.
- 506 [5] A.P. Browning, S.W. McCue, R.N. Binny, M.J. Plank, E.T. Shah, M.J. Simpson.  
507 Inferring parameters for a lattice-free model of cell migration and proliferation  
508 using experimental data. *Journal of Theoretical Biology*. 437 (2018) 251–260.
- 509 [6] A.Q. Cai, K.A. Landman, B.D. Hughes. Multi-scale modeling of a wound-healing  
510 cell migration assay. *Journal of Theoretical Biology*. 245 (2007) 576–594.
- 511 [7] M.H. Chan, P.S. Kim. Modelling a Wolbachia invasion using a slow-fast dispersal  
512 reaction-diffusion approach. *Bulletin of Mathematical Biology*. 75 (2015) 1501–  
513 1523.
- 514 [8] A. Davis, R. Gao, N. Navin. Tumor evolution: Linear, branching, neutral or  
515 punctuated? *Biochimica et Biophysica Acta - Reviews on Cancer*. 1867 (2017)  
516 151–161.
- 517 [9] F.D. di Fagagna, P.M. Reaper, L. Clay-Farrace, H. Fiegler, P. Carr, T. von  
518 Zglinicki, G. Saretzki, N.P. Carter, S.P. Jackson. A DNA damage checkpoint  
519 response in telomere-initiated senescence. *Nature*. 426 (2003) 194–198.

- 520 [10] A. Eladdadi, D. Isaacson. A mathematical model for the effects of HER2  
521 overexpression on cell proliferation in breast cancer. *Bulletin of Mathematical*  
522 *Biology*. 70 (2008) 1707–1729.
- 523 [11] G.I. Evan, K.H. Vousden. Proliferation, cell cycle and apoptosis in cancer.  
524 *Nature*, 411 (2001) 342–348.
- 525 [12] F. Frascoli, B.D. Hughes, M.H. Zaman, K.A. Landman. A computational model  
526 for collective cellular motion in three dimensions: general framework and case  
527 study for cell pair dynamics. *PLOS ONE*. 8 (3), e59249.
- 528 [13] J. García-Algarra, J. Galeano, J.M. Pastor, J.M. Iriondo, J.J. Ramasco.  
529 Rethinking the logistic approach for population dynamics of mutualistic  
530 interactions. *Journal of Theoretical Biology*. 363 (2014) 332–343.
- 531 [14] P. Gerlee. The model muddle: in search of tumor growth laws. *Cancer Research*.  
532 73 (2013) 2407–2411.
- 533 [15] Z. Guan, S. Jia, Z. Zhu, M. Zhang, C.J. Yang. Facile and rapid generation of  
534 large-scale microcollagen gel array for long-term single-cell 3D culture and cell  
535 proliferation heterogeneity analysis. *Analytical Chemistry*. 86 (2014) 2789–2797.
- 536 [16] N.K. Haass, K.A. Beaumont, D.S. Hill, A. Anfosso, P. Mrass, M.A. Munoz,  
537 I. Kinjyo, W. Weninger. Real-time cell cycle imaging during melanoma growth,  
538 invasion, and drug response. *Pigment Cell & Melanoma Research*. 27 (2014) 764–  
539 776.
- 540 [17] P. Haridas, C.J. Penington, J.A. McGovern, D.L.S. McElwain, M.J. Simpson.  
541 Quantifying rates of cell migration and cell proliferation in co-culture barrier  
542 assays reveals how skin and melanoma cells interact during melanoma spreading  
543 and invasion. *Journal of Theoretical Biology*. 423 (2017) 13–25.
- 544 [18] L. Hayflick. The limited *in vitro* lifetime of human diploid cell strains.  
545 *Experimental Cell Research*. 37 (1965) 614–636.
- 546 [19] W. Jin, E.T. Shah, C.J. Penington, S.W. McCue, L.K. Chopin, M.J. Simpson.  
547 Reproducibility of scratch assays is affected by the initial degree of confluence:

548 experiments, modelling and model selection. *Journal of Theoretical Biology*. 390  
549 (2016) 136–145.

550 [20] W. Jin, C.J. Penington, S.W. McCue, M.J. Simpson. A computational  
551 modelling framework to quantify the effects of passaging cell lines. *PLOS ONE*.  
552 12 (2017) e0181941.

553 [21] W. Jin, E.T. Shah, C.J. Penington, S.W. McCue, P.K. Maini, M.J. Simpson.  
554 Logistic proliferation of cells in scratch assays is delayed. *Bulletin of Mathematical*  
555 *Biology*. 79 (2017) 1028–1050.

556 [22] P. Jolicoeur, J. Pontier. Population growth and decline: a four-parameter  
557 generalization of the logistic curve. *Journal of Theoretical Biology*. 141 (1989)  
558 563–571.

559 [23] H. Kaneoka, G. Perez-Rojas, T. Sasasaki, C.J. Benike, E.G. Engleman. Human  
560 T lymphocyte proliferation induced by a pan-T monoclonal antibody (anti-Leu  
561 4): heterogeneity of response is a function of monocytes. *Journal of Immunology*.  
562 131 (1983) 158–164.

563 [24] P.K. Maini, D.L.S. McElwain, D.I. Leavesley. Traveling wave model to interpret  
564 a wound-healing cell migration assay for human peritoneal mesothelial cells. *Tissue*  
565 *Engineering*. 10 (2004) 475–482.

566 [25] P.K. Maini, D.L.S. McElwain, D. Leavesley. Travelling waves in a wound healing  
567 assay. *Applied Mathematics Letters*. 17 (2004) 575–580.

568 [26] J.D. Murray. *Asymptotic analysis*. (2012) Springer Science & Business Media,  
569 New York.

570 [27] J.D. Murray. *Mathematical biology. I: An introduction*, 3rd edn. (2002)  
571 Springer, Heidelberg.

572 [28] J.T. Nardini, D.A. Chapnick, X. Liu, D.M. Bortz. Modeling keratinocyte wound  
573 healing dynamics: cell-cell adhesion promotes sustained collective migration.  
574 *Journal of Theoretical Biology*. 400 (2016) 103–117.

- 575 [29] Z. Neufeld, W. von Witt, D. Lakatos, J. Wang, B. Hegedus, A. Czirok. The  
576 role of Allee effect in modelling post resection recurrence of glioblastoma. *PLoS*  
577 *Computational Biology*. 13(11) (2017) e1005818.
- 578 [30] G.K. Pavlath, D. Thaloor, T.A. Rando, M. Cheong, A.W. English, B. Zheng.  
579 Heterogeneity among muscle precursor cells in adult skeletal muscles with differing  
580 regenerative capacities. *Developmental Dynamics*. 212 (1998) 495–508.
- 581 [31] C.D. Powell, S. López, A. Dumas, D.P. Bureau, S.E. Hook, J. France.  
582 Mathematical descriptions of indeterminate growth. *Journal of Theoretical*  
583 *Biology*. 425 (2017) 88–96.
- 584 [32] V. Pozzobon, P. Perré. Han’s model parameters for microalgae grown under  
585 intermittent illumination: Determined using particle swarm optimization. *Journal*  
586 *of Theoretical Biology*. 437 (2018) 29–35.
- 587 [33] M.N. Read, J. Bailey, J. Timmis, T. Chtanova. Leukocyte motility models  
588 assessed through simulation and multi-objective optimization-based model  
589 selection. *PLOS Computational Biology*. 12(9) (2016) e1005082.
- 590 [34] A. Sakaue-Sawano, H. Kurokawa, T. Morimura, A. Hanyu, H. Hama, H. Osawa,  
591 S. Kashiwagi, K. Fukami, T. Miyata, H. Miyoshi, T. Imamura, M. Ogawa, H.  
592 Masai, A. Miyawaki. Visualizing spatiotemporal dynamics of multicellular cell-  
593 cycle progression. *Cell* 132 (2008) 487–498.
- 594 [35] E.A. Sarapata, L.G. de Pillis. A comparison and catalog of intrinsic tumor  
595 growth models. *Bulletin of Mathematical Biology*. 76 (2014) 2010–2024.
- 596 [36] B.G. Sengers, C.P. Please, R.O. Oreffo RO. Experimental characterization  
597 and computational modelling of two-dimensional cell spreading for skeletal  
598 regeneration. *Journal of the Royal Society Interface*. 4 (2007) 1107–1117.
- 599 [37] L. Sewalt, K. Harley, P. van Heijster, S. Balasuriya. Influences of Allee effects  
600 in the spreading of malignant tumours. *Journal of Theoretical Biology*. 394 (2016)  
601 77–92.
- 602 [38] H. Sheardown, Y.L. Cheng. Mechanisms of corneal epithelial wound healing.  
603 *Chemical Engineering Science*. 51 (1996) 4517–4529.

- 604 [39] J.A. Sherratt, J.D. Murray JD. Models of epidermal wound healing. Proceedings  
605 of the Royal Society Series B. 241 (1990) 29–36.
- 606 [40] M.J. Simpson, K.A. Landman, K. Bhaganagarapu. Coalescence of interacting  
607 cell populations. Journal of Theoretical Biology. 247 (2007) 525–543.
- 608 [41] C.M. Taylor, A. Hastings. Allee effects in biological invasions. Ecological  
609 Letters. (2005) 895–908.
- 610 [42] K.K. Treloar, M.J. Simpson, D.L.S. McElwain, R.E. Baker. Are *in vitro*  
611 estimates of cell diffusivity and cell proliferation rate sensitive to assay geometry?  
612 Journal of Theoretical Biology. 356 (2014) 71–84.
- 613 [43] A. Tsoularis, J. Wallace. Analysis of logistic growth models. Mathematical  
614 Biosciences. 179 (2002) 21–55.
- 615 [44] B.N. Vo, C.C. Drovandi, A.N. Pettitt, M.J. Simpson MJ. Quantifying  
616 uncertainty in parameter estimates for stochastic models of collective cell  
617 spreading using approximate Bayesian computation. Mathematical Biosciences  
618 263 (2015) 133–142.
- 619 [45] W. Wagner, S. Bork, P. Horn, D. Krunic, T. Walenda, A. Diehlmann, V. Benes,  
620 J. Blake, F.X. Huber, V. Eckstein, P. Boukamp. Aging and replicative senescence  
621 have related effects on human stem and progenitor cells. PLOS. ONE. 4 (2002)  
622 e5846.
- 623 [46] G.B. West, J.H. Brown, B.J. Enquist BJ. A general model for ontogenetic  
624 growth. Nature. 413 (2001) 628–631.
- 625 [47] J.M. Willaime, F.E. Turkheimer, L.M. Kenny, E.O. Aboagye. Quantification  
626 of intra-tumour cell proliferation heterogeneity using imaging descriptors of 18F  
627 fluorothymidine-positron emission tomography. Physics in Medicine and Biology.  
628 58 (2013) 187–203.